

SUPPORTING INFORMATION

Electroactive substrates for surface-enhanced Raman spectroscopy based on overgrown gold-nanoparticle arrays by electrodeposition on indium tin oxide

Nerea Gonzalez-Pato,^{a,b} Xavier Rodriguez Rodriguez,^a Nicola Pellizzi,^{a,c} Claudia Fasolato,^d Judith Guasch,^{a,,b,e} Paolo Postorino,^f Jaume Veciana,^{a,b} Alejandro R. Goñi,^{a,f,g} Imma Ratera^{a,b*}*

a. Institut de Ciència de Materials de Barcelona (ICMAB-CSIC), Campus UAB, Bellaterra 08193, Spain

b. CIBER de Bioingeniería, Biomateriales y Nanomedicina (CIBER-BBN), Spain

c. Physics Department, University of Calabria, Ponte P. Bucci cubo 33B,87036 Rende (CS), Italy

d. CNR-ISC, Istituto dei Sistemi Complessi, c/o Sapienza Università di Roma, P.le Aldo Moro 5, 00185 Roma, Italy

e. Dynamic Biomimetics for Cancer Immunotherapy, Max Planck Partner Group, ICMAB-CSIC, Campus UAB, Bellaterra, 08193 Barcelona, Spain

f. Dipartimento di Fisica, Università Sapienza, P.le Aldo Moro 5, 00185 Rome, Italy

g. ICREA, Passeig Lluís Companys 23, 08010 Barcelona, Spain

Surface roughness analysis using AFM of glass covered by gold and by ITO.

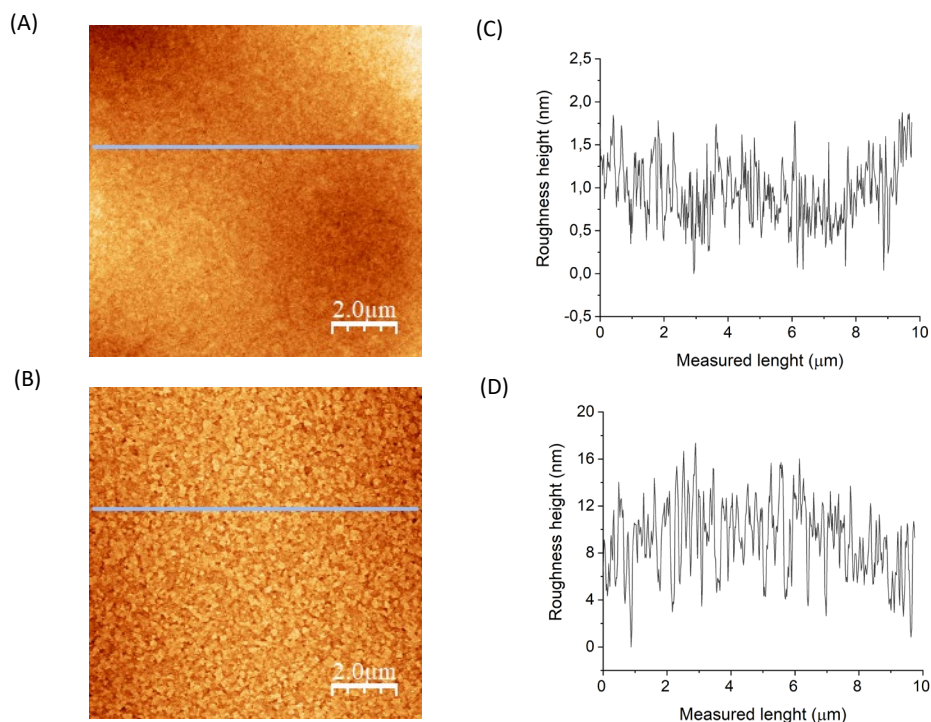


Figure S1. AFM topography image of (A) 200 nm thick layer of gold on glass and (B) ITO on glass substrate with their corresponding roughness profiles along the x axis (blue line), represented in (C) and (D) respectively. RMS= 0.7 nm for gold and RMS= 3.1 nm for ITO

Time dependence of gold growth on ITO substrate, at different voltages.

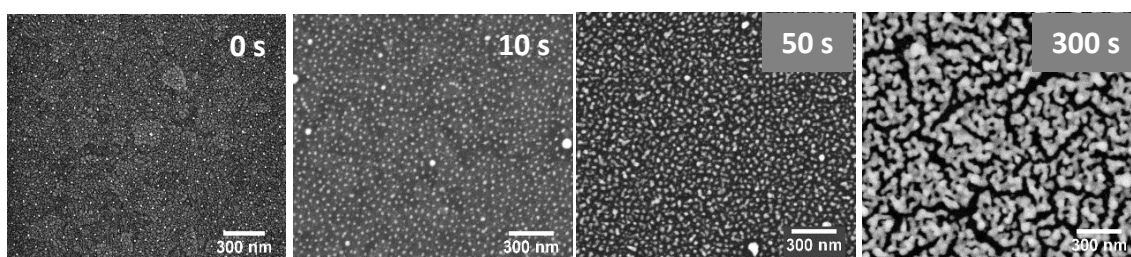


Figure S2. SEM images illustrating Au electrodeposition at a constant voltage (-1.0 V) as a function of deposition time for AuNPs pre-patterned ITO substrate using an aqueous solution of HAuCl₄. Images are displayed in order of increasing times from left to right.

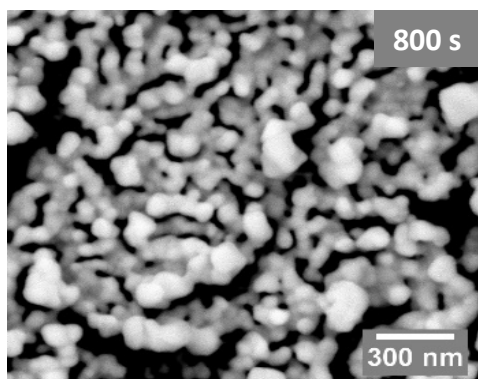


Figure S3. SEM image of AuNPs pre-patterned ITO substrate after electrodeposition of gold during 800 s at -0.6 V using HAuCl_4 aqueous solution.

Gold nanoparticles on ITO for the three different substrates studied in this work.

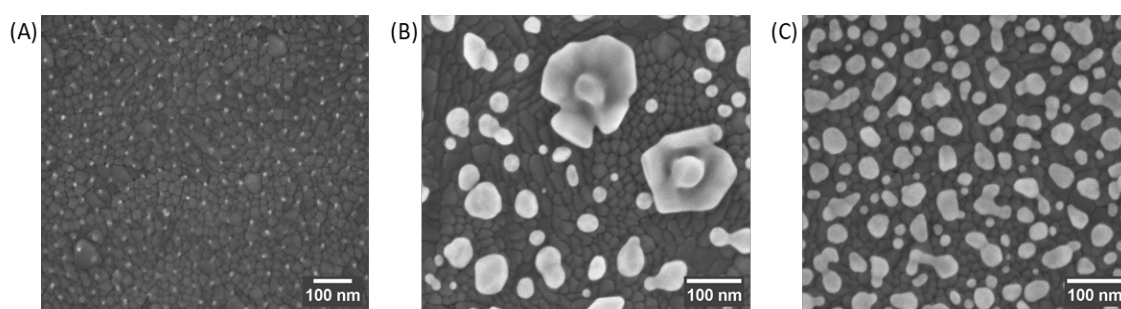


Figure S4. Magnification of SEM images for (A) AuNPs/ITO, (B) Au@ITO and (C) Au@AuNPs/ITO substrates.

For completeness, we refer to the work of Ref. 26 (Y. Hu et al.), where another two-step deposition method is also reported, but different than ours. In the former case, the first nucleation of AuNPs follows by cyclic voltammetry and the subsequent growth of these nanoparticles by applying a constant potential. By doing so, the nucleation step leaves randomly distributed particles. Here is where the BCML plays an important role because it allows us to obtain a pattern on the substrate with well-ordered nanoparticles and homogeneous spacing. In the second step, this is translated into a better homogeneity of the substrate, and, consequently, a more homogeneous SERS signal all over the surface.

Dependence of current on scan rate of the cyclic voltammetry measurements.

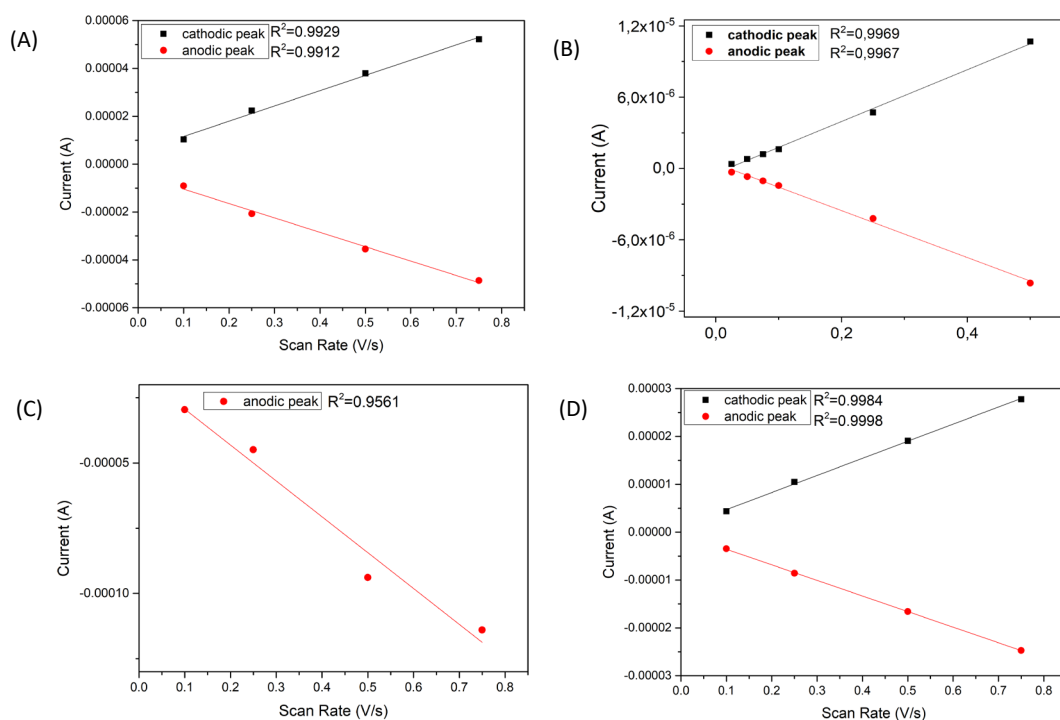


Figure S5. Current vs scan rate plots of cathode and anode peaks of cyclic voltammograms of switchable 11-(ferrocenyl)-undecanethiol SAMs on (A) 200-nm thick bare gold film on glass substrate (Au/Glass), (B) AuNPs on ITO substrates (AuNPs/ITO), (C) Au electrodeposited directly on ITO substrate (Au@ITO) and (D) Au electrodeposited on ITO substrate pre-patterned with AuNPs (Au@AuNPs/ITO). The plots correspond to the evolution of cathodic peaks (black) and of anodic peaks (red).

Surface coverage calculations using the cyclic voltammetry curves.

From the voltammograms in Figure 5 of the manuscript, the fraction of the exposed gold surface covered by the analyte (Γ) has been inferred using Equation (1), where Q is obtained from the peak area divided by the scan rate, n is the number of electrons transferred for the electroactive ferrocene group ($n = 1$), F is the Faraday constant, and A is the area of the electrode immersed in the electrolyte solution. The resulting molecular surface coverages obtained are in agreement with the expected increment of the gold area on each substrate (see Table S1).

$$\Gamma = \frac{Q}{nFA} \quad (1)$$

Table S1. Fraction of the gold surface covered by the switchable 11-(ferrocenyl)-undecanethiol self-assembled monolayer for the different substrates.

NAME	Scan rate	Peak area	Surface coverage	Surf. coverage MEAN	
Units	V/s	A·s	mol/cm ²	mol/cm ²	
Au200nm /Glass	I	0.1	1.02E-06	1.51E-10	
	II	0.25	2.25E-06	1.33E-10	1.15E-10
	III	0.5	2.86E-06	8.46E-11	
	IV	0.75	4.73E-06	9.33E-11	
Au@ITO	I	0.1	3.73E-07	5.52E-11	MEAN
	II	0.25	9.02E-07	5.34E-11	5.19E-11
	III	0.5	1.71E-06	5.07E-11	
	IV	0.75	2.46E-06	4.86E-11	
Au@AuNPs/ITO	I	0.1	2.47E-06	3.65E-10	
	II	0.25	4.45E-06	2.64E-10	4.81E-10
	III	0.5	2.38E-05	7.04E-10	
	IV	0.75	2.99E-05	5.89E-10	

Electrical stability of FcC11SH SAM on the developed SERS-substrate.

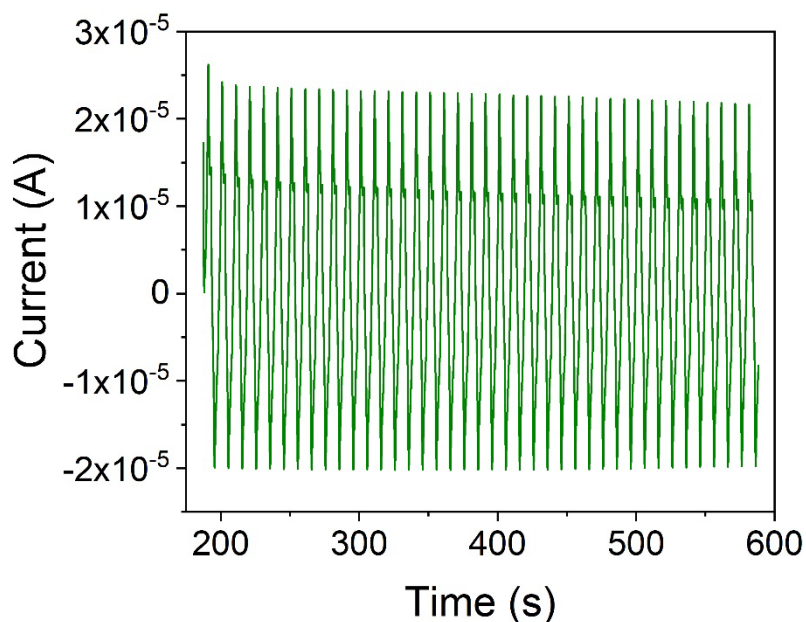


Figure S6. Electrical stability study of the developed conductive Raman-active substrate (Au@AuNPs/ITO) using a switchable 11-(ferrocenyl)-undecanethiol SAM as redox probe and performing 40 switching cycles of oxidation and reduction at a constant scan rate of 0.1 Vs^{-1} .

SERS measurements were performed in the four different substrates to compare their efficiency. In a first attempt, the three available lasers in our lab were tested, resulting the 633 nm laser the best option, as the 532 nm showed a bright luminescence that would influence the background and the 785 nm laser line gave a poor signal. Even though the UV-Vis spectra did not show a plasmon resonance band at a specific wavelength, the 633 nm was chosen because it yielded the best results.

SERS measurements and results.

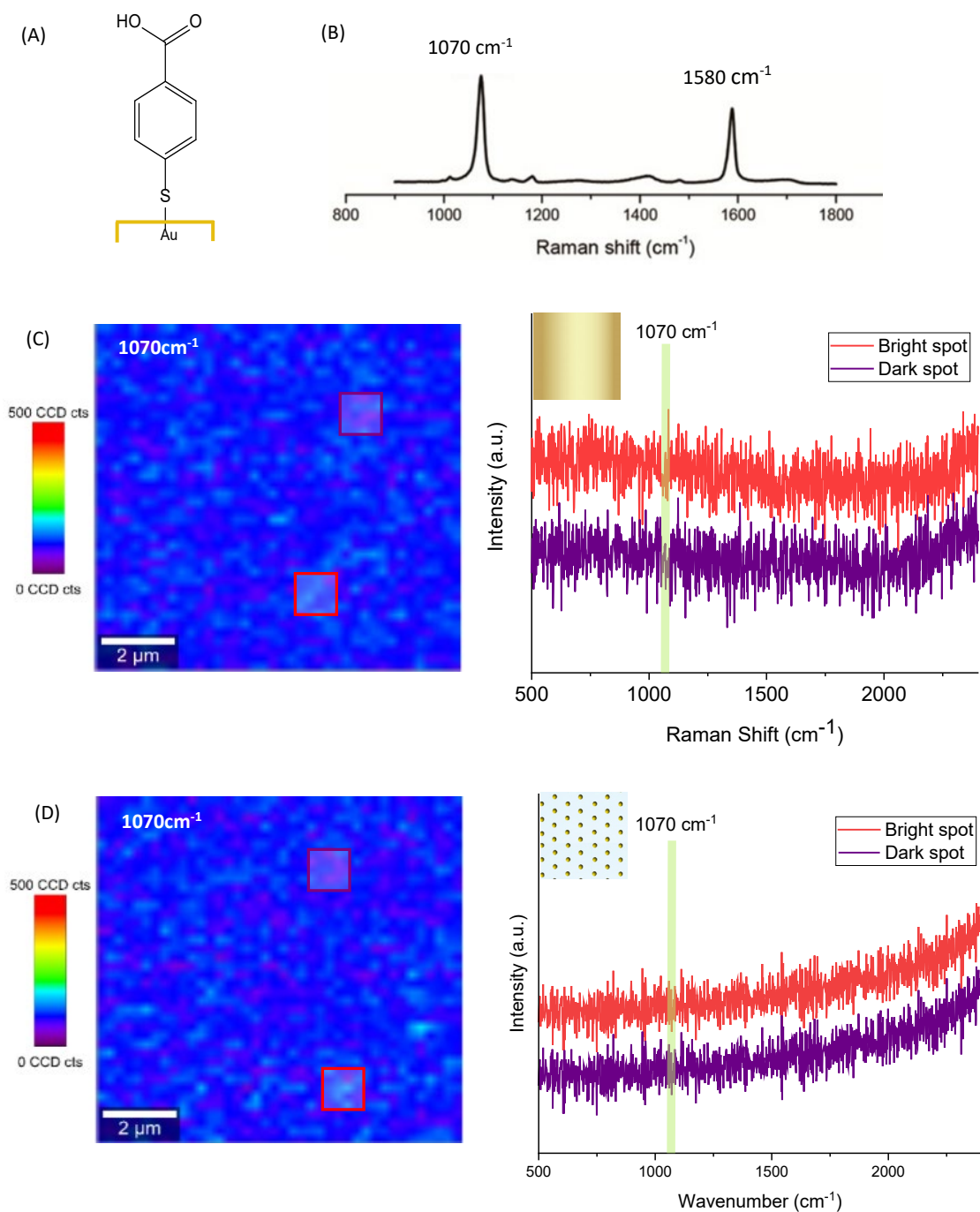


Figure S7. (A) Molecular structure of 4-mercaptobenzoic acid (4-MBA) attached to Au. (B) Raman spectrum of the 4-MBA molecule, with markers on the more intense peaks. (C) Raman intensity map at 1070 cm^{-1} of the bare gold (Au/Glass) substrate and (D) the ITO substrate with AuNPs (AuNPs/ITO substrate). Right panels show two representative

spectra obtained by integrating the Raman signal within the square of the corresponding color. To ease the comparison, all color scales are the same.

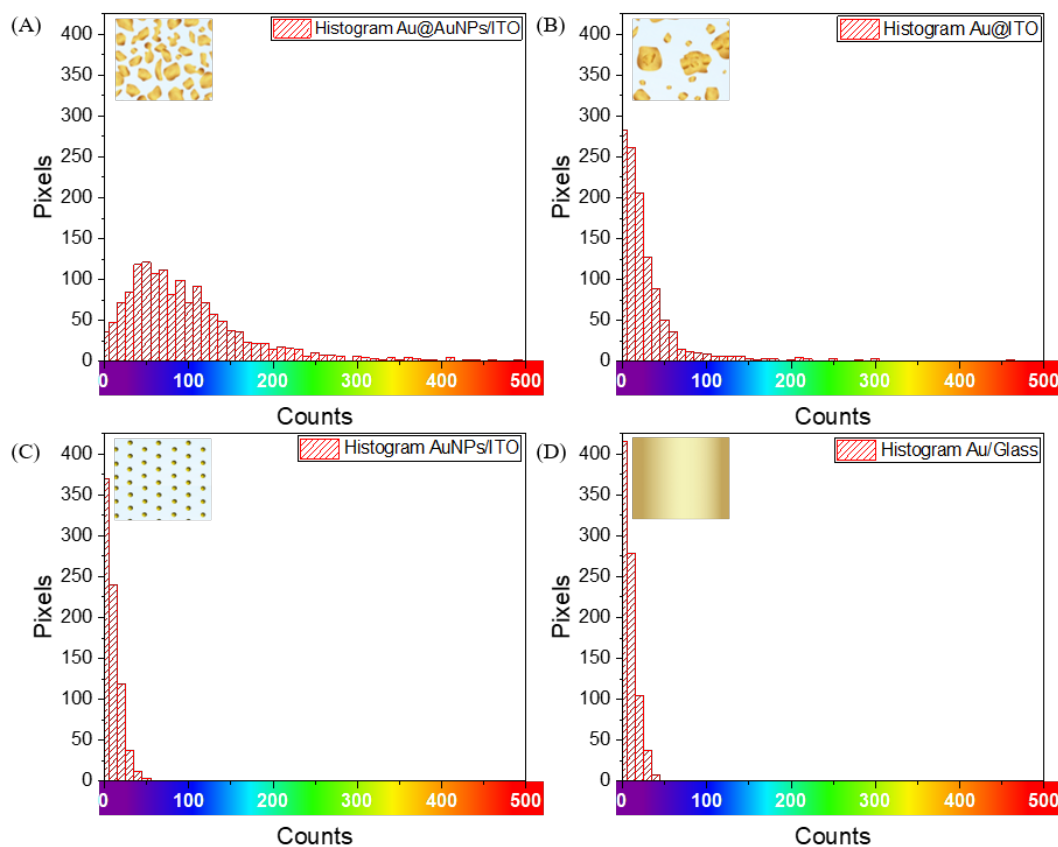


Figure S8. Histograms representing the amount of pixels with the same counts (i.e., Raman intensity) from the SERS maps at 1580 cm^{-1} for the four studied substrates, functionalized with 4-MBA molecules. (A) Au electrodeposited on ITO substrate, prepatterned with AuNPs (Au@AuNPs/ITO). (B) Au electrodeposited directly on ITO substrate (Au@ITO). (C) AuNPs on ITO substrates (AuNPs/ITO). (D) Bare gold 200 nm thick substrate (Au/glass).

The short-, medium- and long-range variability of the SERS enhancement was estimated by spectroscopic mapping. The analysis was carried out on the Au@ITO and Au@AuNPs/ITO substrates, produced using different Au electrodeposition times (600 s and 800 s) directly on ITO and on ITO pre-patterned with AuNP, respectively. In particular, maps with different sampling steps were performed. The short-range variability is estimated considering 1 μm spaced experimental points (i.e., spectra), the medium-range variability considering 10 μm spaced experimental points, the long-range variability considering 100 μm spaced experimental points. The SERS variability was estimated as the ratio between the standard deviation and the average intensity of the 1070 cm^{-1} band over the different datasets (each containing more than 100 experimental points). We express the ratio as a percentage, hence a variability of 100% means that the intensity population shows a large dispersion, about the value of the average intensity. The variability is strongly reduced in the pre-patterned substrates, the 600 s sample showing the best performance.

Table S2. Comparison of the variability of the different substrates studied at 600 s and 800 s for different ranges.

Sample	Electrodeposition time	Short range (1μm) variability	Medium range (10μm) variability	Long range (100μm) variability
Au@ITO	600 s	100 %	57 %	81 %
Au@ITO	800 s	31%	85 %	94 %
Au@AuNPs/ITO	600 s	22 %	34 %	43 %
Au@AuNPs/ITO	800 s	37 %	40 %	46 %

Michael addition reaction on solution followed by cyclic voltammetry.

Before following the Michael addition reaction between benzoquinone and L-cysteine on surface, we have done it in solution. It was possible to see by cyclic voltammetry how the L-cysteine reacts only when a positive voltage is applied, that means all the quinone is in its benzoquinone form (Figure S9 B). In contrast, when negative voltage is applied to the

solution to have all the molecules as hydroquinone (reduced state) the voltammogram remains the same, showing that there is not reaction with the L-cysteine, thus the molecules are still electroactive (Figure S9 C).

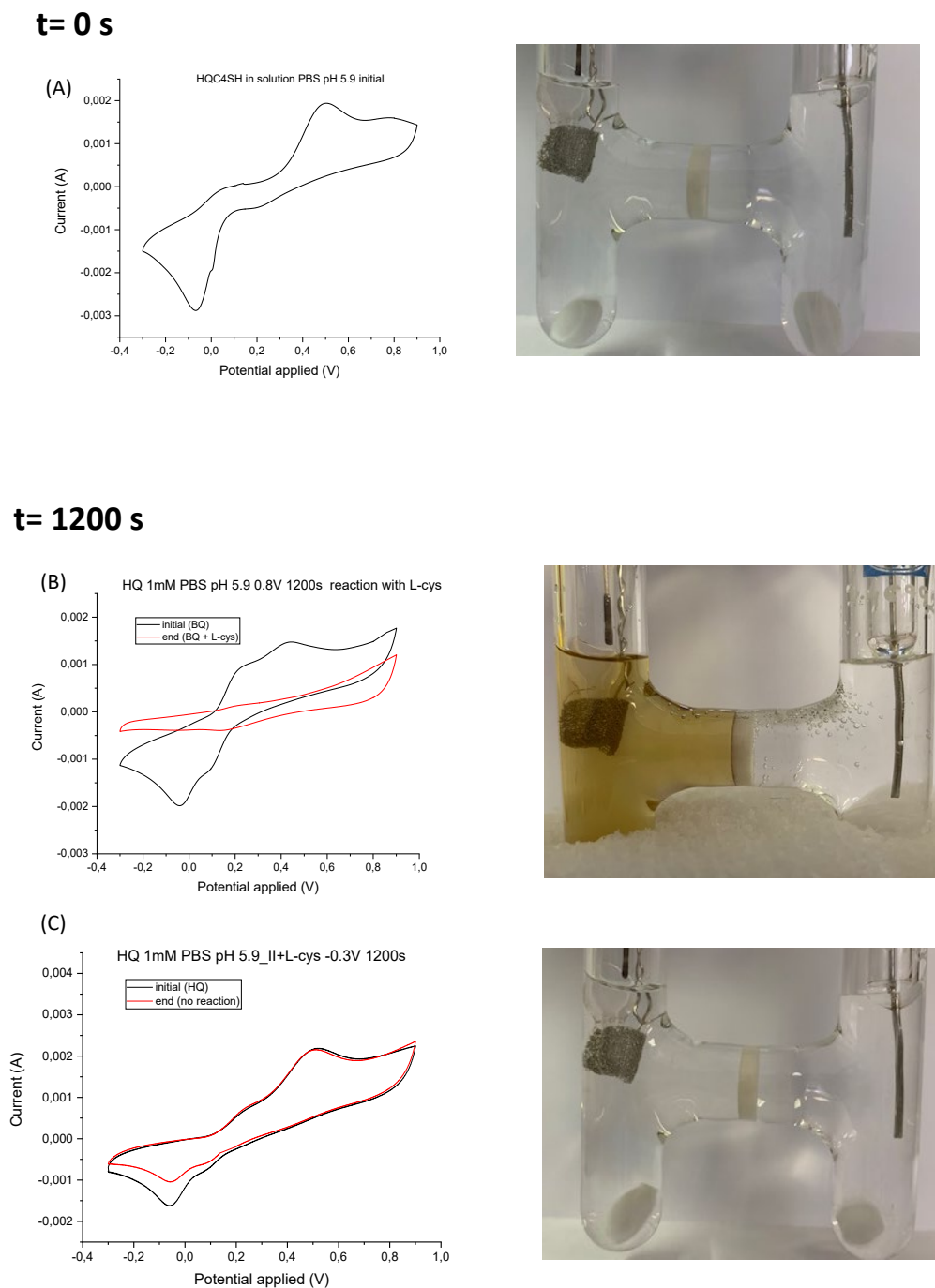


Figure S9. Electrochemical reaction between the L-cysteine and benzoquinone, oxidized from the hydroquinone state in solution. (A) Cyclic voltammogram of the hydroquinone in solution before adding L-cysteine (initial state). (B) Cyclic voltammogram of

benzoquinone under the application of 0.8 V at 0 s (black) and after 1200 s (red) in the presence of L-cysteine. (C) Cyclic voltammogram of hydroquinone after the application of -0.3 V at 0 s (black) and after 1200 s (red) in the presence of L-cysteine.

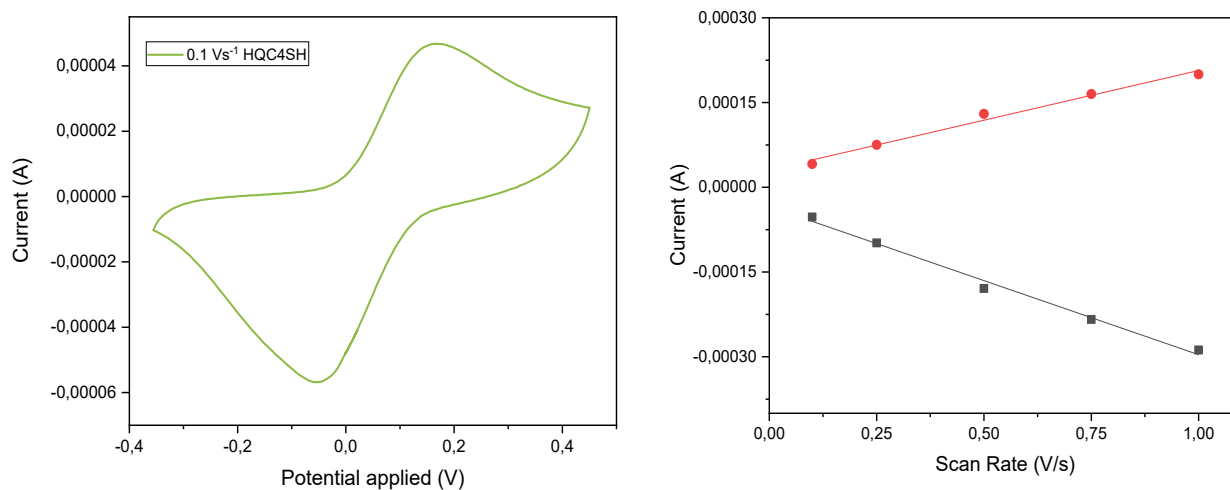


Figure S10. Left: cyclic voltammogram of the Au@AuNPs/ITO surface with a SAM of the thiolated hydroquinone (HQC4SH) molecule, using a 3-electrode setup, Au@AuNPs/ITO substrate was used as working electrode (WE), Pt wire as counter electrode (CE) and Ag/AgCl as reference electrode (RE). The electrolyte used was PBS, at a scan rate of 0.1 Vs⁻¹ Right: Linear dependence of currents with increasing scan rates of the same substrate, from 0.1 Vs⁻¹ to 1 Vs⁻¹.